

Investigation of Influence of Different Fungi on Decaying of White Birch by Electrochemical Fingerprints

Jinneng Wang* and Xuwei An*

College of Architectural Engineering, Chongqing Institute of Engineering, Banan District, 400056, Chongqing, China

*E-mail: wangjn1985@163.com, 02363@cqie.edu.cn

Received: 1 July 2022 / *Accepted:* 9 August 2022 / *Published:* 10 September 2022

Decaying of wood is a complex process, and the study of the mechanism and the changes of chemical substances caused by wood decay can provide a theoretical basis for the selection of decay-resistant construction materials. Electrochemical fingerprinting is a novel analytical technique to determine the signal of electrochemically active substances in a sample. In this work, electrochemical techniques were used to investigate changes in fingerprint profiles of white birch building timber after decay by different wood decay fungi. Combined with infrared spectroscopy, we found that the lignin was degraded to some extent in all wood decay caused by white rot fungi. Although the change of benzene ring skeleton was not obvious, the side chains such as the disease group, CH structure, and phenol ether bond between the benzene rings of lignin had been partially degraded. In contrast, no degradation of lignin was found after decay by brown rot fungi. In addition, all timber had degradation of cellulose and hemicellulose functional groups.

Keywords: Electrochemical fingerprint; White birch; Building timber; Wood corrosion; FTIR

1. INTRODUCTION

As a natural and environmentally friendly material, wood has unique environmental and aesthetic properties that are irreplaceable compared to synthetic materials. As an important renewable resource, the level of comprehensive utilization of wood is related to the sustainable development of the global economy and society [1–3]. In order to use forest resources efficiently and conserve wood scientifically, one of the effective ways is to increase the service life of wood through wood preservation [4]. Wood decay is the gradual change in color and structure of wood due to the invasion of wood-rotting fungi, resulting in the destruction of cell walls and subsequent changes in physical and mechanical properties [5–7].

White rot, brown rot and soft rot caused by fungi are the most damaging to wood. Decay fungi require adequate conditions for growth and reproduction, mainly nutrition, temperature, humidity, air and pH [8,9]. There are also many types of wood decay, and depending on the living state of the wood, wood decay can be divided into live wood decay and non-live wood decay [10]. According to the location where wood decay occurs, it can be further divided into wood white rot and wood brown rot [11–13]. The fungus that causes brown rot in wood is brown rot fungus, which mainly decomposes cellulose and polypentose in wood, but basically does not destroy lignin, and the wood is brown after decay. In brown rot lumber, cellulose can be reduced from about 60% to about 5% and wood weight loss increases. When the weight reduction percentage is greater than 20%, the wood shrinks significantly in the chordal and radial directions [14,15]. White rot fungic cause white rot in wood, mainly decomposing lignin in wood, a small amount of decomposition of cellulose and polypentose. Soft rot is wood decay caused by ascomycetes and hemipterans. This decay is quite common and can occur in many environments. Soft rot breaks down the cellulose of the wood and causes cavities to form in the cell walls of the wood, which is more harmful to the surface of the wood [16].

Nondestructive testing (NDT) is a non-destructive testing technique for wood growth characteristics, physical and mechanical properties and residual defects that gradually emerged in the 1960s. NDT techniques were first applied to the inspection of standing timber, and then gradually applied to the detection of defects in wood components [17,18]. The most commonly used wood non-destructive testing methods are: micro-drilling impedance testing, Pilodyn testing, stress wave testing and ultrasonic testing. Micro-drill inspection uses a wood impedance meter to drill into the wood at a constant rate. As the drilling depth continues to increase, a corresponding resistance variation value is generated, resulting in a depth-dependent resistance curve on the detection path [19–21]. Similar to microdrill impedance testing, Pilodyn testing is based on the principle of shooting a fixed size probe into the wood with a fixed size force, and the depth the probe is shot into the wood is the result of the test [22–25]. The basic principle of stress wave detection is that when a mechanical strike is applied at a point on the surface of the wood, a stress wave propagation is generated within the wood. If there are defects such as decay or cracks in the propagation path of the stress wave, its propagation path will change from a straight line to a curve [26–30]. At the same time, the propagation time will increase accordingly and the propagation speed of the stress wave perpendicular to the direction of the wood grain will increase sharply. Non-metallic ultrasonic inspection to attenuate the mechanical wave intensity to change the direction and path of its own propagation, thereby bypassing the defect interface, so that the condition of internal defects can be determined [31–34].

Electrochemical fingerprinting is a novel analytical technique to determine the signal of electrochemically active substances in a sample. This technique has been used in recent years for the investigation of a variety of plants [35–39]. Since wood decay fungus produce some electrochemically active substances when decomposing wood, it is possible to investigate the electrochemical fingerprinting of wood under different decay conditions to determine the nature of decay. In this work, we investigated the decay experiments of four wood-rotting fungus white birch building timber to determine the biodegradation capacity of each wood-rotting fungus white birch wood. Infrared spectroscopy was used to study the changes in the functional groups of white birch building timber after decay by four species of wood decay fungi. In addition, electrochemical techniques were used to

investigate the changes in fingerprint profiles of white birch building timber after decay by different wood decay fungi.

2. EXPERIMENTAL

2.1. Reagents and instruments

White birch building timber was purchased from local building material market of Chongqing. *Irpex lacteus*, *Piptoporus betulinus*, *Fomes fomentarius* and *Coriolus versicolor* were purchased from GuYan Biotech Co., Ltd.

River sand sawdust preparation: In a 500 mL wide-mouth triangular bottle, add 150 g of washed dry river sand, sapwood sawdust (15 g), corn flour (8.5 g) and brown sugar (1 g), mix well. Separate 3 pieces of feeding wood on the surface, add 100 mL of maltose solution into the bottle slowly, plug the bottle with cotton stopper and wrap the waterproof paper. Sterilize in a steam autoclave (pressure 0.1 MPa, temperature 121°C) for 1 h.

All electrochemistry tests were recorded at a CHI760E working station. A three-electrodes system was applied. A Nicolet Impact-410 infrared spectrometer has been used for recording the infrared spectra of decay sample.

2.2. White birch building timber decay experiment

Fungal mycelium was added to the river sand sawdust medium in 28 °C, air relative humidity of 75% to 85% of the climate chamber incubation until the mycelium grows all over the Petri dish. When the surface is full of mycelium and put into the specimen by the fungal infestation.

White birch building timber was cut into specimens of 5 mm diameter and 5 mm length, and each sample was repeated three times. The specimens were dried at 100°C and subsequently sterilized for 1 h. The samples were kept in a steam sterilizer at atmospheric pressure for 30 min to achieve a moisture content of 40%-60%.

Wood specimens have been prepared and placed in the medium that has grown full of mycelium under aseptic conditions and sealed with sealing film. The specimens were placed in the culture chamber to be infested with the fungus. After decay treatment, the specimens were removed, dried and weighed to remove mycelium and impurities.

2.3. Electrochemical fingerprints and infrared spectra recording

The white birch building timber corroded by 4 decaying fungi was removed, gently scraped off the surface mycelium and impurities, and dried in the oven until constant weight. Gently scrape a little of the decayed and discolored part of the specimen surface with a razor blade and disperse it in alcohol or water. A small amount of the dispersion was dipped coated at the surface of the glassy carbon electrode (GCE) for electrochemical fingerprinting. The electrochemical fingerprint was recorded at a

three-electrode system, where a GCE, a Pt wire and a Ag/AgCl (3M KCl) electrode were used as working electrode, counter electrode and reference electrode, respectively. The electrochemical fingerprint was recorded at either a 0.1 M phosphate buffer solution (PBS, pH 7.0) or a 0.1 M acetic acid buffer solution (ABS, pH 4.5). Linear sweep voltammetry (LSV) was used for electrochemical fingerprint recording. The scan rate is 50 mV/s. The powder was also mixed with KBr crystals under an infrared lamp and ground finely to a starchy consistency, and then a small amount of the finely ground sample was pressed into a transparent sheet on a tablet press for the recording of infrared spectra.

3. RESULTS AND DISCUSSION

We used four wood decay fungi to decay white birch building timber and performed statistical analysis on the weight loss rate (Table 1). The biodegradation times of the four wood decay fungi were different, with a short degradation time for wood with high decay and a total degradation time of 40 to 100 days. The basic features of the weight loss rate of the specimens after biodegradation by wood-rotting fungi showed that *Coriolus versicolor* was the most biodegradable to timber and had the least inter-strain variability. It was followed by *Fomes fomentarius*, but with high interstrain variability. Then *Piptoporus betulinus*, which had less interstrain variation, and *Irpex lacteus*, which had the weakest biodegradability.

Table 1. Weight loss rate of white birch building timber after decaying using *Irpex lacteus*, *Piptoporus betulinus*, *Fomes fomentarius* and *Coriolus versicolor*.

	<i>Irpex lacteus</i>	<i>Coriolus versicolor</i>	<i>Fomes fomentarius</i>	<i>Piptoporus betulinus</i>
Decaying time	100 days	40 days	50 days	90 days
Average weight loss rate (%)	0.3488	0.7033	0.6251	0.5681
Standard deviation	0.08635	0.06815	0.10811	0.08455
Coefficient of variation	24.70	9.68	17.30	14.88
Sample Range	0.54	0.38	0.69	0.64

We then performed infrared spectroscopy on thin sliced specimens of decayed wood after decay of different wood decay fungi. Figure 1A-E shows the infrared spectra of wood powder of the original wood powder and the wood powder of the thin sliced specimens after 120 d of decay by four decay fungi. The changes in the functional groups of the chemical components of the wood samples after degradation by decay fungi can be indicated by the changes in the positions of the spectral peaks and the relative absorption intensities of the absorption peaks in the IR spectra. The absorption peak around 3416

cm^{-1} is due to O-H stretching [40]. The peak around 2931 cm^{-1} can be ascribed to C-H stretching. The absorption peak around 1734 cm^{-1} is due to C=O stretching. The peak around 1507 cm^{-1} is due to aromatic skeletal stretching. The absorption peak around 1457 cm^{-1} is due to C-H deforming in methyl(unsymmetry in -CH and - CH_2) and CH_2 deformation stretching [41]. The absorption peak around 1420 cm^{-1} is due to aromatic skeletal combined with C-H in-plane deforming and stretching. The absorption peak around 1330 cm^{-1} is due to condensation of guaiacyl unit and syringyl unit, syringyl unit and CH_2 bending stretching. The peak around 1245 cm^{-1} is due to C-O-C stretching [42]. The absorption peak around 1161 cm^{-1} is due to C=O stretching. The absorption peak around 1049 cm^{-1} is due to C-O deforming in secondary alcohols and aliphatic ethers [43]. The absorption peak around 898 cm^{-1} is due to C-H stretching out of plane of aromatic rings. The absorption peak around 669 cm^{-1} is due to OH bending stretching out of plane [44].

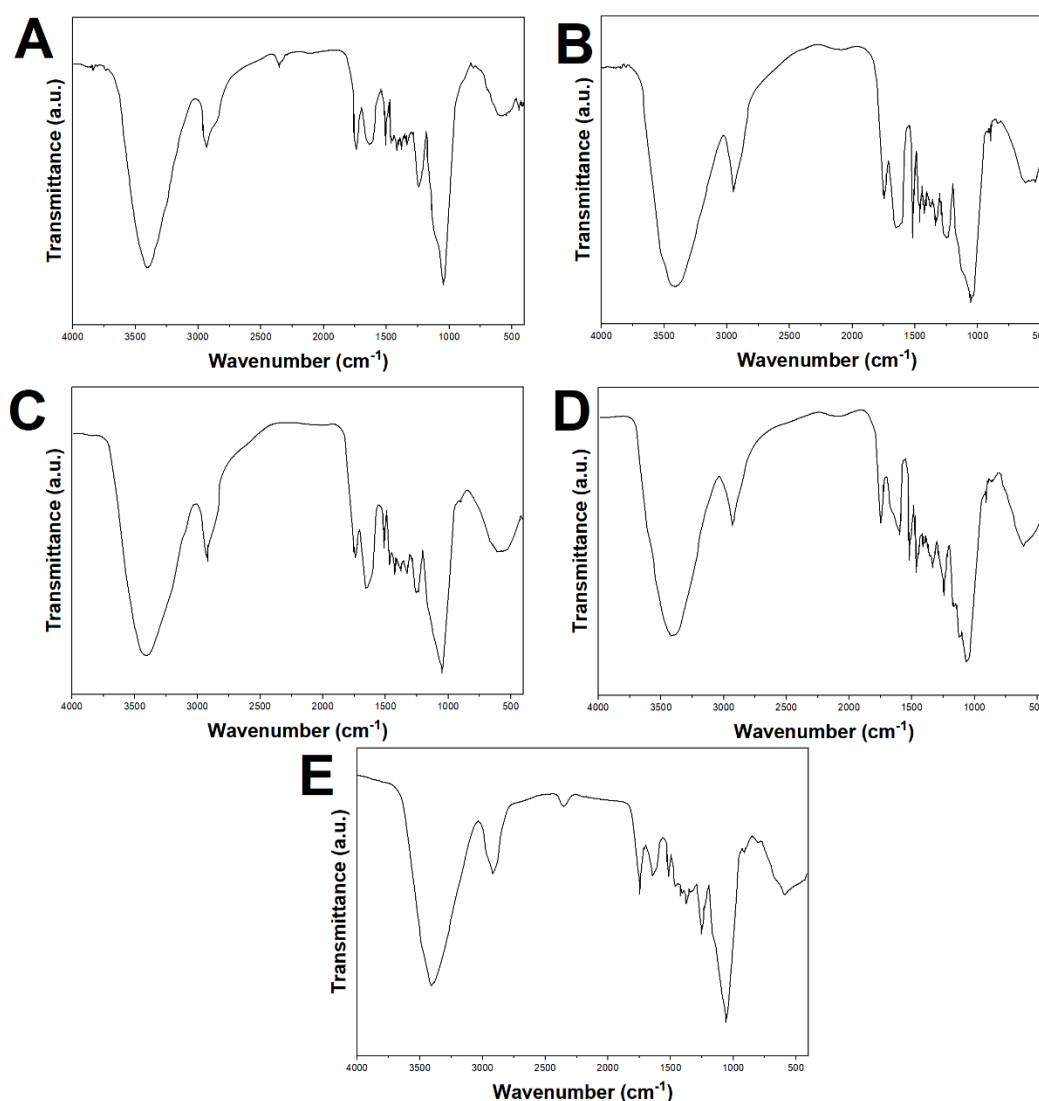


Figure 1. FTIR of (A) raw white birch building timber, (B) *Piptoporus betulinus* decayed specimen, (C) *Fomes fomentarius* decayed specimen, (D) *Coriolus versicolor* decayed specimen, and (E) *Irpex lacteus* decayed specimen.

Figure 2 shows the fingerprints of white birch building timber during the decay. All specimen exhibited peaks, indicating the electrochemical oxidation of substances [45–47]. These substances could be polyphenols, ascorbic acid and ketones [48–50]. However, the amount and type of these substances can vary according to the decaying fungi. Combined with the FTIR results, it is clear from the chemical structure of lignin that the carbon groups of lignin in wood are mainly present in the side chains of structural units. Some of them are aldehyde groups, most of which are located on the γ -carbon atom of the structural unit. The other part is a ketone group, located on the β -carbon atom of the side chain.

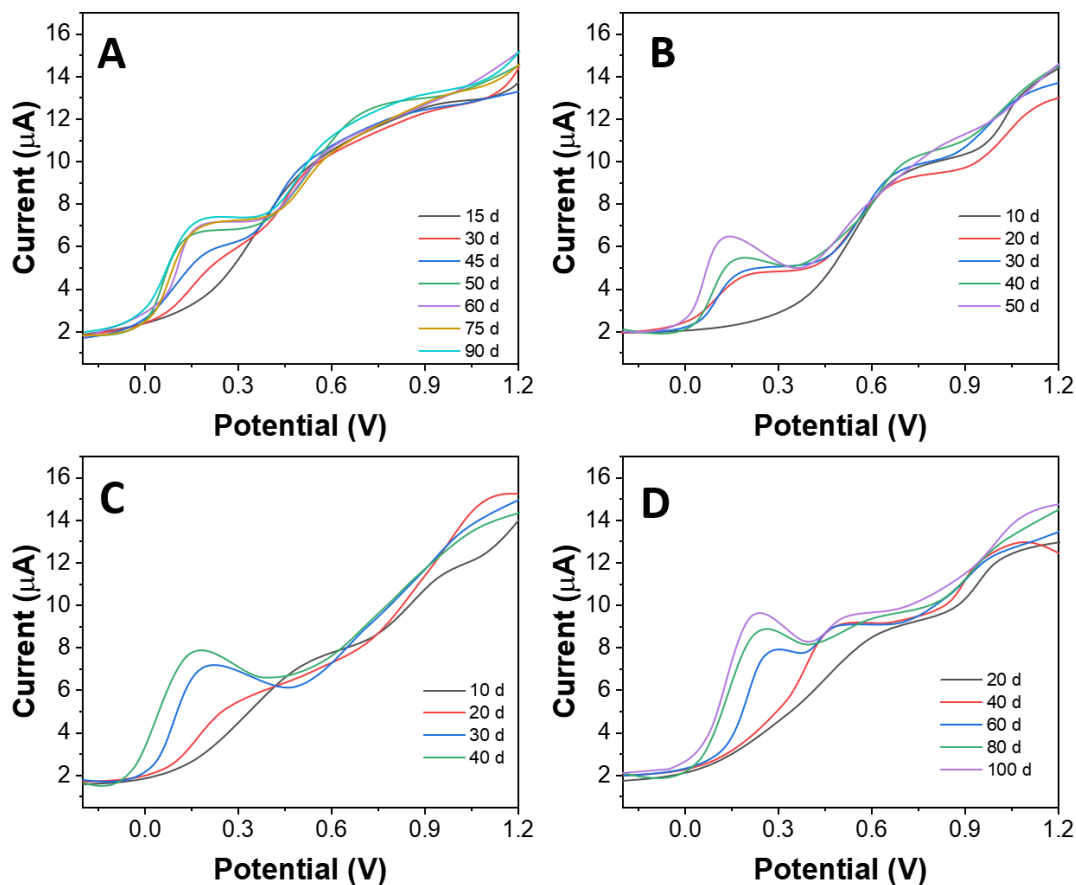


Figure 2. Electrochemical fingerprints of (A) *Piptoporus betulinus* decayed specimen, (B) *Fomes fomentarius* decayed specimen, (C) *Coriolus versicolor* decayed specimen, and (D) *Irpex lacteus* decayed specimen recorded under 0.1 M PBS (pH 7.0).

The absorption peak of the O-H stretching vibration in the hydroxyl group on the lignin side chain of the wood sample after decaying by *Fomes fomentarius*, *Irpex lacteus*, and *Coriolus versicolor* changed significantly compared to the original specimen. The absorption peaks decreased to 3410 cm^{-1} , (3406 cm^{-1} and 3405 cm^{-1} , respectively, suggesting that the hydroxyl groups on the lignin side chain have received decomposition and decreased [51,52]. The absorption peak of specimen after *Piptoporus betulinus* decaying was slightly enhanced, indicating that the hydroxyl groups on the lignin side chain were not decomposed. After *Coriolus versicolor* decaying, the absorption peak characterizing the C-H stretching vibration in the methyl and methylene groups in the wood sample changed and decreased to

2921 cm^{-1} , indicating that the C-H bond in the methyl and methylene groups was broken [53]. The wood samples were degraded by *Piptoporus betulinus*, *Irpex lacteus*, and the absorption peak characterizing the CH_2 deformation vibration in lignin was enhanced [54]. CH_2 was present on the side chain between the benzene rings of lignin, indicating that the lignin side chain was not broken and degraded. DPV curves of four white birch building timber under ABS were also recorded. As shown in Figure 3, the four white birch building timber also exhibited electrochemical activity under ABS. In addition, the behavior under ABS is different from that under PBS. Combined with the FTIR data, the specimens were degraded to some extent by all three white rot fungi. Although the change of benzene bad skeleton was not obvious, the side chains such as carbon group, CH structure and phenol ether bond between the benzene rings of lignin had been partially degraded [55]. And after decay by brown rot fungi, the lignin did not develop on degradation. This is consistent with the decaying nature of white rot fungi and brown rot fungi [56].

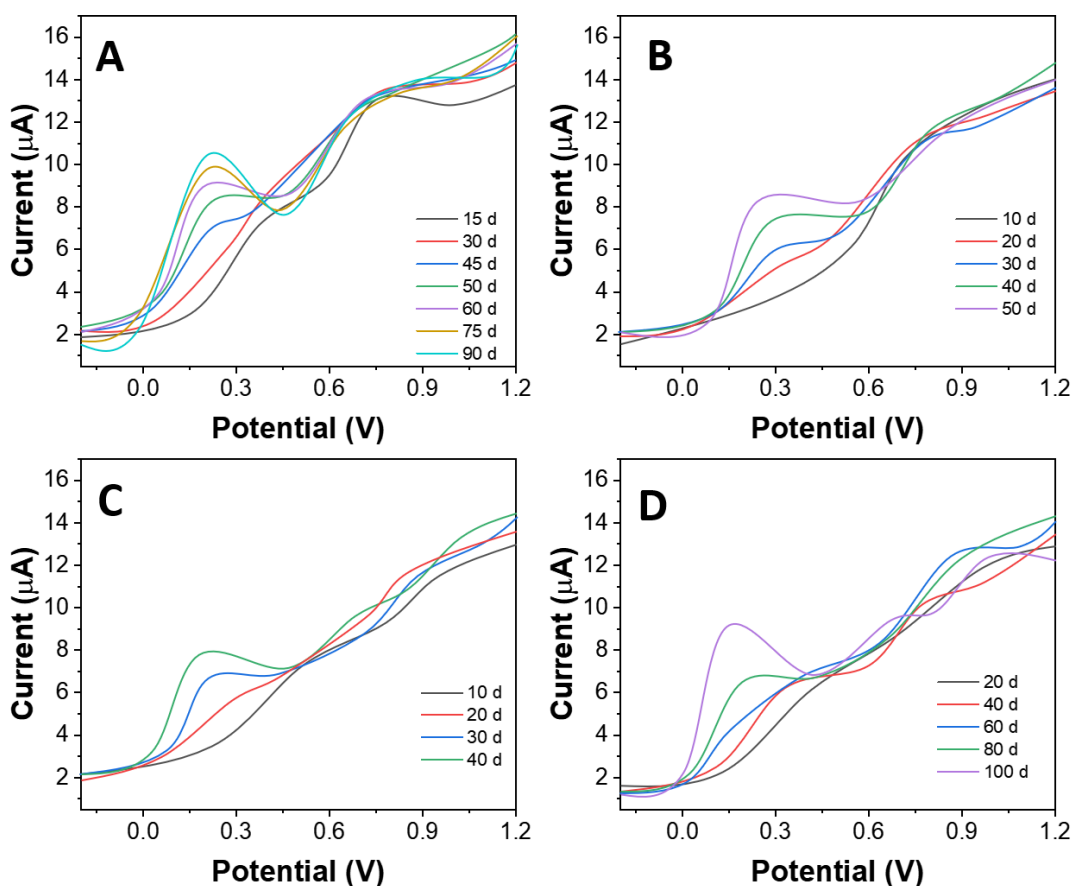


Figure 3. Electrochemical fingerprints of (A) *Piptoporus betulinus* decayed specimen, (B) *Fomes fomentarius* decayed specimen, (C) *Coriolus versicolor* decayed specimen, and (D) *Irpex lacteus* decayed specimen recorded under 0.1 M ABS (pH 4.5).

The magnitude of the changes in the relative absorption intensities of the absorption peaks showed that *Fomes fomentarius* and *Coriolus versicolor* degraded lignin to a greater extent than *Irpex lacteus* degraded lignin. To further understand the compositional changes in white birch building timber

during decay, we examined the changes in heterocellulose, cellulose, hemicellulose, lignin, 1% NaOH extract and benzene-ethanol extract of the specimens during decay of *Fomes fomentarius* (Figure 4).

The measured contents of heterocellulose, cellulose, and hemicellulose were decreasing with increasing decay. The measured contents of lignin and extractives increased, but the relative contents of lignin showed a decreasing trend. This indicates that lignin actually underwent some degradation during brown decay, which was manifested in increasing measured content because its degradation was lower than the mass loss rate [57].

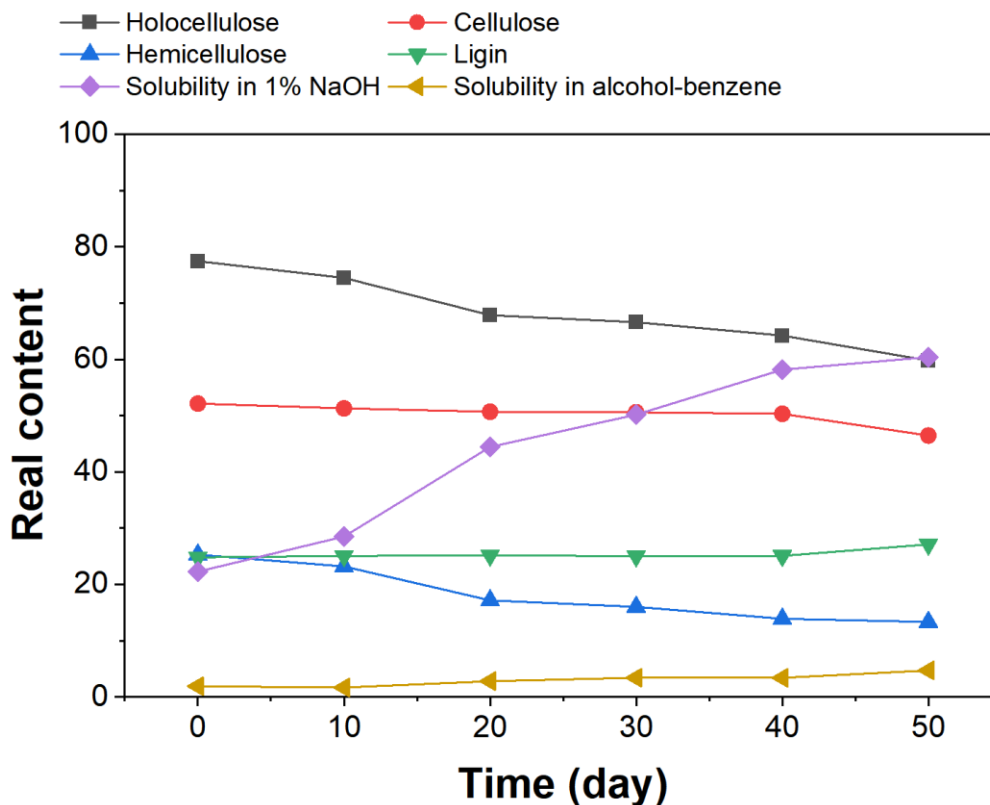


Figure 4. Chemical compositions of white birch building timber with different decay degree.

Analysis of variance (ANOVA) showed that there were overall highly significant differences ($P < 0.01$) in the contents of heterocellulose, hemicellulose, 1% NaOH extracts, and benzene-ethanol extracts in the specimens with different decay levels. The changes of cellulose and lignin contents with the degree of decay were not significant ($P > 0.05$). This indicates that decaying fungus firstly and mainly degrade hemicellulose in wood during brown rot culture, while the decomposition of cellulose and lignin is not significant. Comparing the loss rates of cellulose and hemicellulose, it can be seen that the final losses of hemicellulose and cellulose were 60% and 32%. The rate of loss of hemicellulose content was higher than that of cellulose at all levels of decay. However, the variation of the loss rates of both substances showed that the rate of cellulose loss was significantly faster, while the rate of hemicellulose loss was somewhat slower. This indicates that at this time brown rot fungus begin to break down cellulose

as the mainstay [58]. These patterns of change are determined by the brown rot mechanism of the wood. Because hemicellulose fills between the microfibrils of cellulose in the cell wall of wood, brown rot fungi need to decompose hemicellulose before they can reach cellulose for further decomposition.

4. CONCLUSION

We treated four decay fungi for wood decay on white birch building timber. The decay-treated samples were used for infrared detection and electrochemical fingerprinting. The results showed that *Coriolus versicolor* was the most biodegradable to white birch building timber with the least inter-strain variation. It is followed by *Fomes fomentarius*, but with large interstrain variation. Then there was *Irpex lacteus*, which had less interstrain variation. While *Piptoporus betulinus* had the weakest biodegradability. The degradation rate of wood by *Fomes fomentarius* reached a highly significant positive correlation. *Coriolus versicolor* and *Piptoporus betulinus* reached a highly significant negative correlation in the degradation rate of wood. There was a positive and negative correlation between the degradation rates of wood by three white rot fungi. The degradation rate of wood by brown rot fungi was positively, but not significantly, correlated. This explains the complex relationship between the many wood degradation pathways in each of the two groups, namely, clear rot and brown rot fungi.

References

1. C. Girometta, D. Dondi, R.M. Baiguera, F. Bracco, D.S. Branciforti, S. Buratti, S. Lazzaroni, E. Savino, *Cellulose*, 27 (2020) 6133–6148.
2. C.-Y. Lin, S.-S. Cheng, C.-L. Wu, S.-T. Chang, *Wood Sci. Technol.*, 54 (2020) 237–247.
3. A. Soge, O. Popoola, A. Adetoyinbo, *J. Indian Acad. Wood Sci.*, 15 (2018) 181–189.
4. A.O. Soge, O.I. Popoola, A.A. Adetoyinbo, *Can. J. For. Res.*, 51 (2021) 937–947.
5. O. Hararuk, W.A. Kurz, M. Didion, *For. Ecosyst.*, 7 (2020) 36.
6. S. Gao, X. Yue, L. Wang, *Can. J. For. Res.*, 49 (2019) 145–153.
7. H. Xu, Q. Li, Q. Xu, Z. Bao, L. Wang, T. Xing, *Bioresources*, 14 (2019) 6134–6145.
8. R.M. Jacobsen, A. Sverdrup-Thygeson, H. Kauserud, S. Mundra, T. Birkemoe, *Funct. Ecol.*, 32 (2018) 2571–2582.
9. I. Vandemeulebroucke, S. Caluwaerts, N. Van Den Bossche, *Buildings*, 11 (2021) 134.
10. S.K. Dawson, L. Boddy, H. Halbwachs, C. Bäessler, C. Andrew, T.W. Crowther, J. Heilmann-Clausen, J. Nordén, O. Ovaskainen, M. Jönsson, *Funct. Ecol.*, 33 (2019) 372–387.
11. E.E. Thybring, R. Digaitis, T. Nord-Larsen, G. Beck, M. Fredriksson, *Plos One*, 15 (2020) e0238319.
12. J. Tintner, B. Spangl, F. Reiter, E. Smidt, M. Grabner, *Wood Sci. Technol.*, 54 (2020) 313–327.
13. J.E. Jakes, S.L. Zelinka, C.G. Hunt, P. Ciesielski, C.R. Frihart, D. Yelle, L. Passarini, S.-C. Gleber, D. Vine, S. Vogt, *Sci. Rep.*, 10 (2020) 9919.
14. K. Krause, E.-M. Jung, J. Lindner, I. Hardiman, J. Poetschner, S. Madhavan, C. Matthäus, M. Kai, R.C. Menezes, J. Popp, *PLoS One*, 15 (2020) e0232145.
15. C.L. Goh, R. Abdul Rahim, M.H. Fazalul Rahiman, M.T. Mohamad Talib, Z.C. Tee, *Sens. Actuators Phys.*, 269 (2018) 276–282.
16. N. Macchioni, E. Pecoraro, B. Pizzo, *J. Cult. Herit.*, 30 (2018) 51–56.
17. X. Zheng, E. Cooper, M. Gillott, C. Wood, *Renew. Sustain. Energy Rev.*, 132 (2020) 110049.
18. H. Karimi-Maleh, Y. Orooji, F. Karimi, M. Alizadeh, M. Baghayeri, J. Rouhi, S. Tajik, H.

- Beitollahi, S. Agarwal, V.K. Gupta, *Biosens. Bioelectron.*, 184 (2021) 113252.
19. V. Nagavciuc, Z. Kern, A. Perşoiu, D. Kesjár, I. Popa, *Dendrochronologia*, 49 (2018) 110–117.
 20. C. Brischke, S. Stricker, L. Meyer-Veltrup, L. Emmerich, *Holzforschung*, 73 (2019) 445–455.
 21. H. Karimi-Maleh, A. Khataee, F. Karimi, M. Baghayeri, L. Fu, J. Rouhi, C. Karaman, O. Karaman, R. Boukherroub, *Chemosphere*, 291 (2021) 132928.
 22. S. Di Lella, R. Tognetti, N. La Porta, F. Lombardi, T. Nardin, R. Larcher, *J. Wood Chem. Technol.*, 39 (2019) 90–110.
 23. Y. Fukasawa, K. Matsukura, *Sci. Rep.*, 11 (2021) 8972.
 24. M. Gómez-Hernández, K.G. Ramírez-Antonio, E. Gándara, *Fungal Ecol.*, 39 (2019) 109–116.
 25. H. Karimi-Maleh, F. Karimi, L. Fu, A.L. Sanati, M. Alizadeh, C. Karaman, Y. Orooji, *J. Hazard. Mater.*, 423 (2022) 127058.
 26. S.-J. Pang, G.Y. Jeong, *J. Korean Wood Sci. Technol.*, 47 (2019) 40–50.
 27. X. Yue, L. Wang, J.P. Wacker, Z. Zhu, *PeerJ*, 7 (2019) e6444.
 28. J.D. Castaño, J. Zhang, J.S. Schilling, *J. Microbiol. Methods*, 145 (2018) 10–13.
 29. E.E. Thybring, M. Kymäläinen, L. Rautkari, *Wood Sci. Technol.*, 52 (2018) 297–329.
 30. H. Karimi-Maleh, M. Alizadeh, Y. Orooji, F. Karimi, M. Baghayeri, J. Rouhi, S. Tajik, H. Beitollahi, S. Agarwal, V.K. Gupta, S. Rajendran, S. Rostamnia, L. Fu, F. Saberi-Movahed, S. Malekmohammadi, *Ind. Eng. Chem. Res.*, 60 (2021) 816–823.
 31. M. Jomura, R. Yoshida, L. Michalčíková, V. Tláškal, P. Baldrian, *J. Fungi*, 8 (2022) 673.
 32. G. Beck, *Forests*, 11 (2020) 650.
 33. H. Karimi-Maleh, C. Karaman, O. Karaman, F. Karimi, Y. Vasseghian, L. Fu, M. Baghayeri, J. Rouhi, P. Senthil Kumar, P.-L. Show, S. Rajendran, A.L. Sanati, A. Mirabi, *J. Nanostructure Chem.*, 12 (2022) 429–439.
 34. H. Karimi-Maleh, H. Beitollahi, P.S. Kumar, S. Tajik, P.M. Jahani, F. Karimi, C. Karaman, Y. Vasseghian, M. Baghayeri, J. Rouhi, *Food Chem. Toxicol.* (2022) 112961.
 35. Q. Wang, B. Fan, D. Li, Z. Xu, L. Fu, A. Wang, Y. Zheng, J. Zhu, *Int. J. Electrochem. Sci.*, 16 (2021) 210427.
 36. W. Ye, Y. Zheng, P. Zhang, B. Fan, Y. Li, L. Fu, *Int J Electrochem Sci*, 16 (2021) 211041.
 37. Y. Zheng, X. Li, F. Han, L. Fu, J. Sun, *Int J Electrochem Sci*, 16 (2021) 211136.
 38. L. Fu, Y. Zheng, A. Wang, P. Zhang, S. Ding, W. Wu, Q. Zhou, F. Chen, S. Zhao, *J. Herb. Med.*, 30 (2021) 100512.
 39. Y. Xu, Y. Lu, P. Zhang, Y. Wang, Y. Zheng, L. Fu, H. Zhang, C.-T. Lin, A. Yu, *Bioelectrochemistry*, 133 (2020) 107455.
 40. M. Couturier, S. Ladeveze, G. Sulzenbacher, L. Ciano, M. Fanuel, C. Moreau, A. Villares, B. Cathala, F. Chaspoul, K.E. Frandsen, *Nat. Chem. Biol.*, 14 (2018) 306–310.
 41. K.J. Vössing, E. Niederleithinger, *Holzforschung*, 72 (2018) 467–476.
 42. L. Zhang, A. Tiemann, T. Zhang, T. Gauthier, K. Hsu, M. Mahamid, P.K. Moniruzzaman, D. Ozevin, *Eur. J. Wood Wood Prod.*, 79 (2021) 335–347.
 43. A. Can, S. Palanti, H. Sivrikaya, B. Hazer, F. Stefani, *Cellulose*, 26 (2019) 5075–5084.
 44. B. Oberle, K. Ogle, A.E. Zanne, C.W. Woodall, *PloS One*, 13 (2018) e0196712.
 45. Y. Zheng, D. Wang, X. Li, Z. Wang, Q. Zhou, L. Fu, Y. Yin, D. Creech, *Biosensors*, 11 (2021) 403.
 46. D. Wang, D. Li, L. Fu, Y. Zheng, Y. Gu, F. Chen, S. Zhao, *Sensors*, 21 (2021) 8216.
 47. B. Fan, Q. Wang, W. Wu, Q. Zhou, D. Li, Z. Xu, L. Fu, J. Zhu, H. Karimi-Maleh, C.-T. Lin, *Biosensors*, 11 (2021) 155.
 48. J. Zhou, Y. Zheng, J. Zhang, H. Karimi-Maleh, Y. Xu, Q. Zhou, L. Fu, W. Wu, *Anal. Lett.*, 53 (2020) 2517–2528.
 49. M. Chen, H. Yang, Z. Song, Y. Gu, Y. Zheng, J. Zhu, A. Wang, L. Fu, *Phyton-Int. Exp. Bot.*, 90 (2021) 1507–1518.
 50. H. Shi, L. Fu, F. Chen, S. Zhao, G. Lai, *Environ. Res.*, 209 (2022) 112747.

51. E.D. Tomak, D. Ustaomer, M.A. Ermeýdan, S. Yildiz, *Measurement*, 127 (2018) 187–197.
52. M. Mubarak, H. Militz, S. Dumarçay, P. Gérardin, *Wood Sci. Technol.*, 54 (2020) 479–502.
53. G. Beck, E.E. Thybring, L.G. Thygesen, *Int. Biodeterior. Biodegrad.*, 135 (2018) 62–70.
54. M. De Angelis, M. Romagnoli, V. Vek, I. Poljanšek, P. Oven, N. Thaler, B. Lesar, D. Kržišnik, M. Humar, *Ind. Crops Prod.*, 117 (2018) 187–196.
55. V. Cristini, J. Tippner, P. Nop, J. Zlámá, M. Hassan Vand, V. Šeda, *Holzforchung* (2022) in-press.
56. J. Dahlen, L. Schimleck, E. Schilling, *Forests*, 11 (2020) 479.
57. B.N. Marais, P.B. van Niekerk, C. Brischke, *Forests*, 12 (2021) 698.
58. C.W. Woodall, V.J. Monleon, S. Fraver, M.B. Russell, M.H. Hatfield, J.L. Campbell, G.M. Domke, *Sci. Data*, 6 (2019) 180303.

© 2022 The Authors. Published by ESG (www.electrochemsci.org). This article is an open access article distributed under the terms and conditions of the Creative Commons Attribution license (<http://creativecommons.org/licenses/by/4.0/>).